

Upgrade of the Infrared Camera Diagnostics for the JET ITER-like wall Divertor^{a)}

I. Balboa,¹ G. Arnoux,¹ T. Eich², B. Sieglin², S. Devaux², W. Zeidner², C. Morlock³, U. Kruezi³, G. Sergienko³, D. Kinna¹, P.D. Thomas¹, M. Rack³ and JET EFDA Contributors*

JET-EFDA, Culham Science Centre, Abingdon, OX14 3DB, UK

¹*EURATOM/CCFE Fusion Assoc., Culham Science Centre, Abingdon, OX14 3DB, UK*

²*Max-Planck-IPP, EURATOM Association, D-85748 Garching, Germany*

³*Institut für Energie und Klimaforschung Plasmaphysik, Forschungszentrum Jülich GmbH, EURATOM Association FZJ, D-52425 Jülich, Germany*

* *See the Appendix of F. Romanelli et al., Proceedings of the 23rd IAEA Fusion Energy Conference 2010, Daejeon, Korea*

(Presented XXXXX; received XXXXX; accepted XXXXX; published online XXXXX)

(Dates appearing here are provided by the Editorial Office)

For the new ITER-like Wall (ILW) at JET, two new infrared diagnostics (KL9B, KL3B) have been installed. These diagnostics can operate between 3.5-5 μ m and up to sampling frequencies of ~20kHz. KL9B and KL3B image the horizontal and vertical tiles of the divertor. The divertor tiles are tungsten coated carbon fibre composite (CFC) except the central tile which is bulk tungsten and consists of lamella segments. The thermal emission between lamellae affects the surface temperature measurement and therefore KL9A has been upgraded to achieve a higher spatial resolution (by a factor of 2). A technical description of KL9A, KL9B and KL3B and cross correlation with a near infrared (NIR) camera and a 2-color pyrometer is presented.

I. INTRODUCTION

Infrared thermography is an essential tool in measuring the surface temperature and estimating the heat loads on the JET divertor target tiles. With the construction of the ITER-like wall (ILW) at the JET tokamak, two new infrared diagnostics, referred to as KL9B and KL3B have been installed which are located at octants 8 and 4 respectively. KL9B views from the top, mainly the central tile and KL3B images the inner and outer vertical tiles. The KL9B and KL3B cameras are technical twins of one existing diagnostic called KL9A¹. KL9A and KL9B both image the divertor central tiles at different toroidal locations, allowing the study of toroidal asymmetries.

II. OVERVIEW of KL3B, KL9A AND KL9B

KL9A/B and KL3B are three IR diagnostics dedicated to the study of temperatures and heat loads on the divertor region. The central tile, #5, consists of four stacks denoted as 'A', 'B', 'C' and 'D'. The infrared cameras used in these diagnostics have all been manufactured at FLIR ATS (<http://www.flir.com>). Therefore, they all share the following features for the camera sensor: size (320x256 pixels), pixel pitch (30 μ m) and the sensor's wavelength response is 1.5-5.0 μ m. The ADC resolution is 14 bits. The sampling frequency can go up to 20 kHz depending on the size of the image frame. As an example, for a full frame, the maximum frequency is 383 Hz. However, reducing the window frame enables increasing the sampling frequency (e.g. 96 x 16 pixels corresponds to 10.7 kHz). The integration time can go down up to 3-4 μ s and depends on the imaging system performance. Typical values for KL9B is 10-20 μ s, around 70-100 μ s for KL9A and 400-500 μ s for KL3B. The spatial resolution, is determined by the optics. The optical configuration

for KL9A/B is the same *i.e.* the plasma light is imaged through a set of vacuum sapphire windows and directed by a beam splitter positioned at 45° into the camera. The distance between the divertor and KL9A/B systems is ~5500 mm. Due to the proximity of the KL9A/B cameras to the poloidal field coils (P2 and P3), each camera is enclosed in a magnetic shielding made of 30 mm soft iron. Regarding, the imaging systems for KL9A/B, they both use a beam splitter and a camera lens but with different specifications. For KL9A, the beam splitter is a neutral density filter made of quartz with a reflectivity of 19% in the IR. For KL9B, the beam splitter is a dichroic mirror which enhances the reflectivity to 80% since for KL9B it was possible to optimize the splitter response to the IR range. In turn, this offers the advantage of decreasing the exposure time and therefore it allows the study of fast plasma events such as filaments. At the start of the experimental campaign, KL9A/B had the same lens which had a 100 mm focal length (F/2), with a spectral bandwidth between 3.5-5 μ m. Currently, this is the camera lens used in the KL9B system only. Due to the segmentation of each of the stacks in the central tile into lamellae strips, the gaps in between act also as a hot source. Therefore, in order to estimate more accurately the heat loads around the edges of individual lamellae, a new camera lens was incorporated to KL9A. The KL9A lens has a 200 mm focal length instead but the same F-number (*i.e.* F/2). The spectral bandwidth covers the same range as the one for KL9B and their transmission is very similar (within 2%). A comparison between the fields of view for KL9B and KL9A is given in figure 1. KL9B covers mainly tile #5 and partially tiles #4 and #6. On the other hand, KL9A shows smaller field of view since the lens provides a higher magnification (x2) than KL9B's lens. Consequently, the spatial resolution of KL9A is higher (0.8 mm/pixel) than for KL9B (1.6 mm/pixel). Since the separation

^{a)}Contributed paper published as part of the Proceedings of the 19th Topical Conference on High-Temperature Plasma Diagnostics, Monterey, California, May, 2012.

^{b)}Author to whom correspondence should be addressed:
itziar.balboa@ccfe.ac.uk

between lamellae is 1mm, the increase in spatial resolution allows an increased accuracy in the estimation of the heat fluxes on the lamellae area (5.5mm x 61mm) and the study the effect of parasitic light coming from the gaps, which can affect the KL9B system.

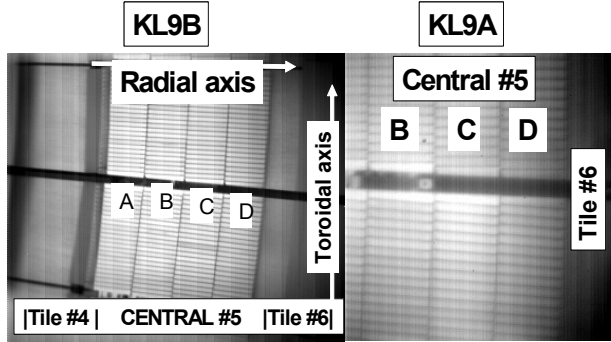


FIG. 1. Fields of view of KL9B and KL9A respectively

KL3B is mounted vertically in front of an endoscope (~2000 mm long) and views the divertor via a 45° mirror located in between the camera and the endoscope window. The 45° mirror is elliptical and it consists of a pyrex substrate and a protected gold coating (67 mm x 47 mm x 11 mm). At the “plasma end” of the endoscope there is a prism which divides the field of view into two sections: in the upper section, tiles #1, #3, #4 and #5 are shown, whereas in the lower section, tiles #7 and #8 are displayed (see figure 2). On the image, both sections are divided by a black line from the prism tilted around ~15°. The distance from the prism to each divertor section shown in figure 2 is different: ~3400 mm for tiles #3, #4 and #5 and ~2500 mm for tiles #7 and #8. This also affects the spatial resolution: ~4.0 mm/pixel for tiles #3, #4 and #5 and ~10.0 mm/pixel for tiles #7 and #8. The imaging system for KL3B consists of three lenses inside the endoscope as well as two doublets in front of the camera. All three IR cameras have an optical filter in front of the sensor. The filter dimensions are 25.4 mm diameter and 1 mm thickness. The filter for KL9A is a low pass type centered at 4.2 ±0.1 μm. For KL9B and KL3B, the filters are of a bandpass type centred at 3.9±0.1 μm with a bandwidth of 1.6 μm and 3.55±0.1 μm with a bandwidth of 0.9 μm respectively. The specifications of the filters were determined by the optical system performance and the temperature range (500°-1500°C) which, in turn, minimizes the contributions from reflections at lower temperatures.

III. CALIBRATION

The main calibration, which was performed in the lab, was carried out using a black body source (diameter: 20 mm, emissivity: 0.99). The source was calibrated between 200°-1200°C. The digital levels were averaged within a selected region of interest (ROI) and measured every 100°C. A measurement of the laboratory’s background light levels was also taken, to remove any spurious contribution. The conversion from digital levels to temperature is obtained by inverting directly the Planck’s equation¹ (1):

$$I(\lambda) = \varepsilon(\lambda) \cdot \frac{2c}{\lambda^4 \cdot \left(e^{\frac{hc}{\lambda k_B T}} - 1 \right)} \quad (1)$$

where ε is the emissivity, λ is the wavelength, c the speed of light, k_B is the Boltzmann constant and T depicts the temperature in Kelvin.

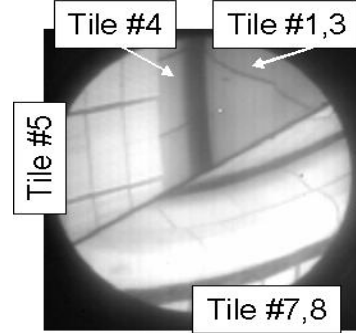


FIG. 2. Field of view of KL3B

This expression is only valid in the case where reflections are considered negligible. Furthermore, the optical response of the entire system needs to be taken into account. The transmission factor for the vacuum window in the KL9B system for 3.9 μm (filter’s wavelength, see section II) is 0.74. As for the optical response of the KL3B endoscope optics for 3.55 μm (designed wavelength, see section II) is 0.04. The tungsten emissivity for these wavelengths is ~0.2². For the results shown on figures, 3, 4 and 5, the contribution from the background has been accounted by measuring the digital levels from frames taken before the plasma and later being subtracted from the data. In addition, the thermocouples embedded in the divertor tiles are used to provide the starting temperature.

IV. RESULTS

The verification of the temperature measurements of the KL9B and KL3B diagnostics was performed by cross comparing the measurements with other, independently calibrated thermal diagnostics. In particular, the ones used for the protection of the plasma facing components inside the vessel, such as near infrared (NIR) cameras and pyrometers. The details of these systems are described in reference 2. Sharing the same vacuum window with KL9B, there are two NIR cameras and four 2-colour pyrometers. The field of view of the NIR cameras covers the same area as KL9B. As a result, one of these cameras (KL2D-P8TB) has been used to cross correlate the measurements from KL9B. Figure 3 shows a profile of the maximum surface temperature within the selected ROI as a function of time of the KL9B and the NIR camera (KL2D-P8TB). The NIR camera is a CCD camera with a band pass filter of 980±10 nm. Due to the high temporal sampling of KL9B, the temperature transients due to the ELMs are recorded whereas the NIR protection camera, which is much slower (50 Hz) does not show this. A smooth curve for KL9B which represents the baseline of the curve has been added for the comparison. The NIR camera temperature range starts at 850°C. Thus, this camera only produces a “real” measurement once this temperature has been reached. The error bars, due to both camera noise and calibration errors, are ±50°C. The calibration errors arise from uncertainties in the transmission responses of the optical components. There is a good agreement between the two cameras (above 850° C). A close up view into a short time window has been added to the graph to show the two temperature profiles.

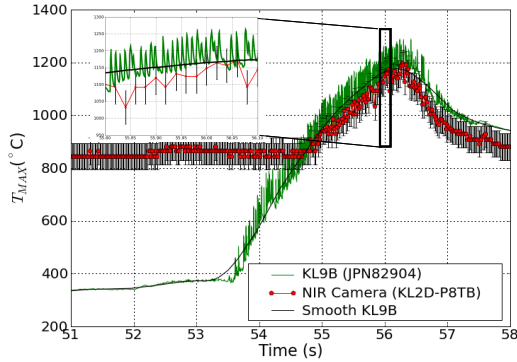


FIG. 3. Comparison of KL9B and NIR camera (KL2D-P8TB). Notice that the NIR camera only starts measuring from 850° C

Regarding the pyrometers, these are 2-colour devices that can operate between 350°-1300° C. The operating wavelengths are $1530\pm 98.5\text{nm}$ and $1660\pm 32.5\text{nm}$. The advantage of 2-colour wavelength pyrometers is that they are independent of the emissivity. The pyrometers measure over an area of 15 mm diameter and give an average temperature over this area (versus time). They can be affected by reflections unless, you are measuring the temperature in areas where the heat flux is sufficiently high (*e.g.* strike line region). One of the four 2-colour pyrometers which shares the same vacuum window with KL9B, has been used to cross compare the temperature with KL9B. The pyrometer's name is KL2D-P8PB. The KL2D-P8PB is centred on lamella #13 on stack C. Thus, its measuring area also partially covers lamellae #12 and #14. Figure 4 shows a reasonable agreement between the pyrometer and KL9B (using a ROI centred at the same spot but without including the gaps between the lamellae) within $\pm 60^\circ\text{C}$ except for the cooling phase. The pyrometer disk covers partially the gaps which have a different emissivity and this might affect the pyrometer measurements during the cooling down. Finally, a comparison between temperature measurements from KL9B and KL3B cameras is shown in figure 5. The maximum temperature as a function of time is given for three pulses (JPN 82630, 82631 and 82643) for KL9B and KL3B. Note that the difference between the two systems is $\pm 50^\circ\text{C}$ and this corresponds to $\sim 2\sigma$ of a total number of measurements of 22,140. The scattering of temperature measurements is larger at higher temperatures (above 800° C) and this might be attributed to several reasons, such as toroidal asymmetries due to the difference in location between the two diagnostics (see section I), also the difference in spatial and temporal resolution (see section II) and finally the viewing angle (it is slightly tangential for KL3B and perpendicular for KL9B). The graphs include the ohmic, NBI heating and cooling phase. For the three pulses, the ELMs can be detected for temperatures above 600° C. Reflections from other sources are not considered significant for the pulses shown, since the ROIs for KL3B and KL9B have been centred around the strike line region (*i.e.* high heat flux) on the divertor tiles.

V. CONCLUSIONS

A technical description of two new IR diagnostics, KL9B and KL3B as well as a comparison of their performance with independently calibrated diagnostics such as a NIR camera and a 2-colour pyrometer is presented. The agreement between KL9B diagnostic and the NIR camera was within $\pm 50^\circ\text{C}$, and with the 2-colour pyrometer the agreement was within $\pm 60^\circ\text{C}$.

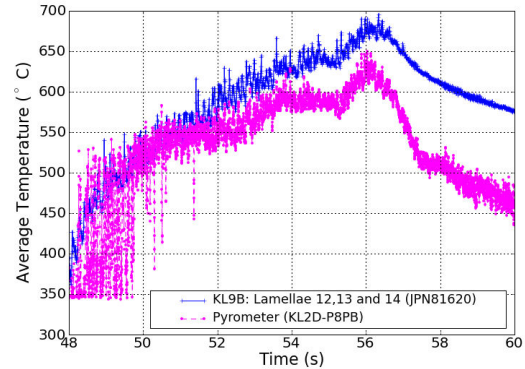


FIG. 4. Comparison of the average temperature between KL9B and 2-color pyrometer (KL2D-P8PB) (see text for ROI size)

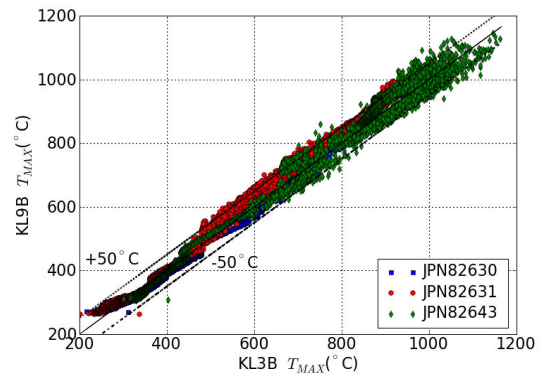


FIG. 5. Comparison of KL9B versus KL3B temperatures for pulses #82630, #82631 and #82643

The measurement of the maximum surface temperature shown in the results was performed within a ROI on the strike line region and for these cases the contribution of reflections was considered negligible. However, in cases where for example the contribution from non thermal emission sources such as Bremstrahlung is significant or when measuring areas of relatively low heat flux, then reflections need to be accounted for in the calculation of the surface temperature. Finally, the thermal emission from the gaps between the lamellae in the central divertor tile has driven the requirement for an upgrade to the KL9A system to increase its spatial resolution and improve the accuracy of the heat fluxes around the edges of the lamellae.

VI. ACKNOWLEDGMENTS & REFERENCES

This work, supported by the European Communities under the contract of Association between EURATOM and CCFE was carried out within the framework of EFDA. The views and opinions expressed herein do not necessarily reflect those of the European Commission. Special thanks to J. Wilson, I. Pearson, R. Fenn and C. Rose for their support during the mechanical design assembly modifications and installations.

¹T. Eich *et al.*, "Type-I ELM power deposition profile with and temporal shape in JET", *Journal of Nuclear Materials*, **415**, S856-S859 (2011)

²G. Arnoux *et al.*, "A protection system for the JET ITER-like wall based on imaging diagnostics" (submitted for this conference)